ROYAL SOCIETY OF CHEMISTRY

COMMUNICATION

Check for updates

In situ thermal fabrication of copper sulfide–polymer hybrid nanostructures for tunable plasmon resonance†

Jing Peng, Bo Zheng, Shuyue Jia, Jingru Gao and Dongyan Tang [ID] *

Here, a novel strategy for fabricating plasmonic-polymer hybrid nanostructures *via* the *in situ* thermal synthesis of copper sulfide (CuS) nanocrystals within poly(*N*-vinyl caprolactam)-based microgels is presented. In particular, the carboxyl groups inside the microgels enriched Cu^{2+} ions *via* electrostatic interaction, which further facilitated the nucleation inside the microgel matrix. The increase in nanocrystals' sizes with more added precursors indicated nanocrystals' continuous growth. The plasmon resonances in CuS nanocrystals were obtained due to the high-density free carriers in the covellite CuS. Both the sizes and the plasmon resonances of the as-synthesized CuS nanocrystals could be modulated by adjusting the amount of precursor. The fabricated hybrid nanostructures possessed good temperature responsivity, adjustable loading capacity, good colloidal stability, and pH dependent plasmon resonance. Furthermore, effective photothermal conversion performance was obtained under the illumination of a 980 nm NIR laser for controlling the phase transition of microgels, revealing promising potential in remotely controlled release of drugs.

Localized surface plasmon resonance in semiconductor nanocrystals has obtained increasing attention in the past ten years owing to their ability to alter light–matter interactions and extensive application in sensors, catalysis and biomedicine.[1] In contrast to the LSPR in metal nanoparticles, which can only be tuned in the visible spectrum by controlling the size and shape and composition, the LSPR in semiconductors nanocrystals can also be regulated *via* the alteration of doping concentration, generating broader optical response from the visible to the far-infrared region. Up to now, various plasmonic semiconductors have been researched, including metal oxides such as molybdenum oxide and metal chalcogenides such as copper sulfide. In particular, copper sulfide nanocrystals have been widely

studied and have found extensive applications in the fields of sensors, therapy and imaging due to their low cost, low toxicity, and intrinsic plasmonic properties.[2,3]

Synthesis and modification are the two most important issues for copper sulfide nanocrystals to fit practical applications. The most used method, *i.e.* colloidal synthesis, can result in high crystallinity and monodispersity of copper sulfide nanocrystals, and complex post-synthesis treatments usually are needed for further application.[4] Hydrothermal/solvothermal methods also have been extensively applied as other alternatives, where polymers such as polyethylene glycol (PEG) or polyvinyl pyrrolidone (PVP) usually act as a stabilizer or surface modifier.[5,6] The use of such polymers can facilitate the formation of colloidally stable plasmonic-polymer hybrid structures. Besides, polymers can further offer smart characteristics since they respond to external stimuli such as ions, pH and temperature, which could significantly enlarge the application of inorganic nanoparticles.[7–9]

Particularly, polymers with thermal responsivity, such as poly(*N*-isopropyl acrylamide) (PNIPAM) or poly(*N*-vinyl caprolactam) (PVCL), can undergo reversible collapse/swelling structure transition in response to changes in temperature, and have been widely studied as smart biomaterials.[10,11] Meanwhile, using microgels as flexible nanoreactors to synthesize inorganic nanoparticles also has been broadly reported.[12] Thus, thermoresponsive microgels can be some of the powerful candidates as reactors to fabricate polymer–nanocrystal hybrid structures. Lots of semiconductor nanocrystals have been synthesized with thermoresponsive microgels as reactors, such as ZnS,[13] CdS,[14,15] and ZnO.[16] However, most of these semiconductor nanocrystals have unobvious or do not have any plasmonic response, and only show absorption within the UV-vis region. In recent years, a heat treatment strategy using PNIPAM-based microgels as reactors has been reported to synthesize plasmonic CuS nanocrystals for near-infrared triggered photothermal therapy.[17] In our work, the heating method has been further developed by simply adding ethanol to water during the synthesis process to avoid the collapse of microgels

School of Chemistry and Chemical Engineering, Harbin Institute of Technology, No. 92, Xidazhi Street, Nangang District, Harbin, Heilongjiang, China. E-mail: dytang@hit.edu.cn

and to further improve the microgels' thermoresponsivity. The final fabricated hybrid microgels exhibited better colloidal stability, distinct temperature responsibility and good plasmon resonance.

The present microgels were synthesized *via* a modified precipitation copolymerization of *N*-vinyl caprolactam and methacrylic acid (MAA) (see the Experimental section), denoted as poly(VCL-*co*-MAA). The ionization degree and pH responsibility are presented in Fig. S1 and S2,† respectively. Previous studies have showed that the phase transition temperature of poly(*N*-vinyl caprolactam) microgels decreases a little with the addition of ethanol and then rapidly increases with the further addition of ethanol due to the higher solubility of PVCL in ethanol than that in water.[18,19] In Fig. S3,† we further confirm that at various pH values and under the treatment of mixed solvents of water and ethanol, the phase transition temperatures of microgels could increase to over 70 °C.

On the basis of that, the synthesis process of CuS nanocrystals was designed as follows. First, the carboxyl groups inside microgels were fully deprotonated at a pH of 7.00. Then Cu^{2+} ions were added dropwise, followed by the addition of ethanol and S^{2-} ions. Finally, the dispersion was sealed and treated at 70 °C under stirring for 12 h. The amount of Cu^{2+} ions was kept at a feeding molar ratio (–COOH : Cu^{2+}) of 2 : 1 and the water/ethanol volume ratio was set as 1 : 1 to maintain the swelling state of microgels.

The as-synthesized product shown in Fig. 1a and S4† was named poly(VCL-*co*-MAA)@CuS1. Fig. 1a shows the existence of spherical structures, filled with large amounts of nanocrystals. The nanocrystal sizes were observed to be 3–10 nm, based on

the observation from Fig. 1b and S5a.† Almost no crystals can be found outside the microgels, which indicated the occurrence of crystal formation inside the microgels. Considering the relatively low content of the nanocrystals within the microgels, high resolution TEM (HRTEM) and selected area electron diffraction (SAED) measurements were used to roughly identify the nanocrystal structures, as shown in Fig. 1b and S5b,† respectively. From the detected results, it seems that the nanocrystals have a lattice spacing of 0.23 nm, corresponding to the (4 2 2) plane of low chalcocite. And the Bragg peaks from SAED were at 0.46 nm and 0.25 nm, possibly corresponding to the (2 1 1) plane and (1 4 2) plane of low chalcocite, consistent with the result of HRTEM. Dynamic light scattering measurements of poly(VCL-*co*-MAA)@CuS1 in Fig. 1c show an average hydrodynamic diameter of 498 nm without the occurrence of any freely dispersed nanocrystals, which also supported the viewpoint that the crystal formation occurred inside the microgels.

Except the synthesis conditions at a relatively high temperature of 70 °C, the present heat synthesis method is similar to the common *in situ* precipitation reaction method within microgels.[20] Usually, Cu^{2+} ions are supposed to be enriched inside negatively charged microgels due to electrostatic interactions. The relatively high temperature favored the crystal formation, including the processes of nucleation and growth. It can be inferred that prior nanocrystal nucleation occurs inside the microgels, rather than outside the microgels. This assumption inspired us to add larger amounts of Cu^{2+} ions than that of the carboxyl groups.

So, a series of hybrid microgels were synthesized with varying feeding Cu^{2+}/–COOH molar ratios of 6 : 2, 10 : 2 and
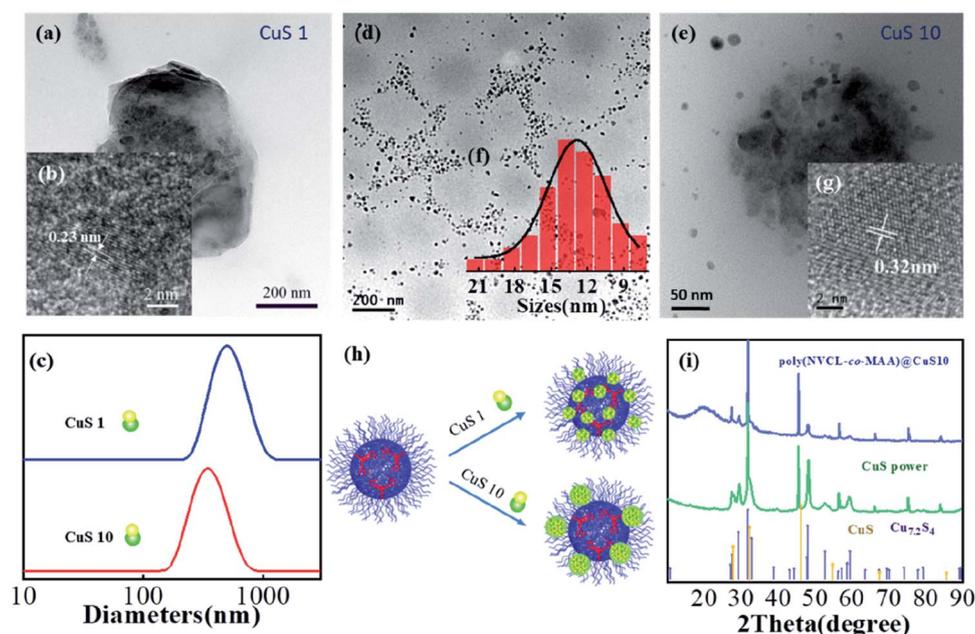

Fig. 1   TEM (a) and HRTEM (b) images of poly(VCL-*co*-MAA)@CuS1 hybrid microgels; (c) hydrodynamic diameter distribution for both hybrid microgels; TEM image (d and e), the size distribution of CuS nanocrystals (f) and HRTEM images (g) of poly(VCL-*co*-MAA)@CuS10 hybrid microgels; (h) the illustration of the formation of poly(VCL-*co*-MAA)@CuS1 and poly(VCL-*co*-MAA)@CuS10 hybrid microgels; (i) XRD pattern of poly(VCL-*co*-MAA)@CuS10 hybrid microgels.

20 : 2, and the samples were thus denoted as poly(VCL-co-MAA)@CuS3, poly(VCL-co-MAA)@CuS5 and poly(VCL-co-MAA)@CuS10, correspondingly. The detailed synthesis parameters are presented in Table S1.†

The microstructures of poly(VCL-co-MAA)@CuS10 hybrid microgels were observed by TEM. Fig. 1d and e show the spherical structures of the microgels, similar to that of poly(VCL-co-MAA)@CuS1. The differences in diameters for the two hybrid microgels were observed in the DLS measurement (Fig. 1c), which mainly originated from the crosslinking effect of the higher loading amount of nanocrystals, as previous studies reported.[21] Furthermore, a large amount of flake-like nanocrystals could be found near the outer shell of the microgels with an average size of 13.04 nm (Fig. 1f), indicating the growth of nanocrystals mainly on the shell of microgels. The HRTEM image (Fig. 1g) presents a lattice spacing of 0.32 nm, possibly corresponding to the (1 0 1) plane of chalcocite CuS. As illustrated in Fig. 1h, the crystal sizes were larger than that in the case of poly(VCL-co-MAA)@CuS1, which indicated the continuous growth of nanocrystals with the addition of more amounts of CuS precursor. These results were similar to other heat synthesis methods.[1]

The structures of poly(VCL-co-MAA)@CuS10 hybrid microgels were identified by X-ray diffraction (XRD) and HRTEM. The XRD result is shown in Fig. 1i. The broad peak at the small angle range of 20 degrees could be corresponded to the amorphous structure of the organic component. Other X-ray diffraction peaks showed a similar pattern to that of CuS powder, which was synthesized via a similar procedure except for the addition of microgels. These peaks can be mainly indexed as hexagonal CuS (JCPDS file number 06-0464), along with a low content of cubic $Cu_{7.2}S_4$ (JCPDS file number 24-0061). The calculated sizes of nanocrystals from the diffraction peak were identified to be 18.1 nm, consistent with the size from the TEM image. The contents of nanocrystals were measured by energy dispersive X-ray spectroscopic analysis (shown in Fig. S6†). Considering the relatively high contents of Cu and C elements within Cu grids, the calculated contents of CuS nanocrystals were based on the detected amounts of S and N atoms. According to that, the percentage content of nanocrystals appeared to be 2.5 wt%. Furthermore, surface elemental analysis was performed using X-ray photoelectron spectroscopy (XPS), and the results are presented in Fig. S7.† The high resolution spectrum of Cu atoms (Fig. S7b†) showed that the fitted peaks at 932.2 and 952.3 eV can well correspond to Cu(I) species for covellite CuS, consistent with a previous reference.[22] And two other peaks at 934.3 and 954.8 eV might be the Cu(I) species for cubic $Cu_{7.2}S_4$. The calculated percentage content of Cu(I) species for covellite CuS was 83.5%, which suggested that most of the inorganic components could be identified as covellite CuS. Besides, the high resolution spectrum of S atoms is shown in Fig. S7c,† and the signal intensity at 162.9 eV suggested the possible existence of S(−1) atoms of covellite, which was close to the result of a previous study.[22] The relatively weak signal could hardly precisely identify the valence of S elements, while a recent study[23] has given evidence that the average valence of S elements of covellite was −1.

As illustrated in Fig. 2a, the localized carboxyl groups inside the microgels played an important role in the enrichment of metal ions, and further facilitated the nucleation and continuous growth of nanocrystals.

The thermoresponsivities of the as-synthesized poly(VCL-co-MAA)@CuS10 hybrid microgels were investigated. As presented in Fig. S8,† at a pH value of 5.85, the transmittance underwent a significant decrease as the temperature increased above 35 °C. With the increase of pH values, the cloud points of the hybrid microgels moved to higher temperatures due to the further ionization of carboxyl groups at higher pH values. These results significantly differed from a previous reference, where the absence of ethanol during the heat-synthesis process of CuS nanocrystals caused relatively poor thermoresponsivity for the hybrid microgels.[17] Additionally, the photograph in Fig. 2b demonstrates that the color of the hybrid microgels was almost unchanged and precipitation cannot be observed even after 14 days, indicating the relatively excellent colloidal stability.

UV-vis-NIR absorption spectra of poly(VCL-co-MAA)@CuS1, 3, 5, and 10 hybrid microgels were recorded, and are presented in Fig. 2c. The poly(VCL-co-MAA)@CuS10 hybrid microgels exhibited a well-defined NIR absorption peak at 965 nm owing to the high-density free carriers in covellite CuS nanocrystals, as well as the low content of $Cu_{7.2}S_4$ nanocrystals. As recent studies suggested, $Cu_{7.2}S_4$ nanocrystals, similar to covellite CuS, also showed good NIR absorption.[24,25] Besides, when the content of CuS precursors reduced by 50% or 70%, the absorbance peaks for the as-synthesized poly(VCL-co-MAA)@CuS5 and poly(VCL-co-MAA)@CuS3 hybrid microgels were red-shifted from 965 nm to 1050 nm and 1188 nm, respectively. As per the result discussed in Fig. 1, the addition of more precursors could cause the increase of nanocrystal size, along with higher free carrier density in nanocrystals.[1] In this way, the decrease in nanocrystal sizes would inversely result in decreased free carrier density in CuS nanocrystals, and further caused the red-shift of the absorption spectra. Besides, the addition of Cu^{2+} ions also affected the pH value of the medium, which might change the absorption spectra of CuS nanocrystals (which would be discussed in the next section). When the content of CuS precursors reduced to 10%, the poly(VCL-co-MAA)@CuS1 hybrid microgels showed unobvious absorption in the vis-NIR region, which might be attributed to the difference in crystal forms, as discussed above.

The effect of pH value on the nanocrystal synthesis was investigated by adding an acid or base. The acid or base was added after exchanging Cu^{2+} ions with microgels to minimize the effect of pH on the enrichment of Cu^{2+} ions within microgels. The detailed discussion about the pH variation and the UV-vis spectrum obtained during the experimental procedure are presented in Fig. S9.† When the pH of the precursor solutions was adjusted to 2.78, 4.94 and 5.20, the final products were found at the pH values of 3.81, 4.59 and 4.87, respectively. And all these three samples exhibited the absorbance peak in the NIR region, as shown in Fig. 2d. For poly(VCL-co-MAA)@CuS10a, with the addition of acid, the absorbance peak was observed at 1080 nm, which was red-shifted from the peak at 965 nm for the poly(VCL-co-MAA)@CuS10 sample, along with
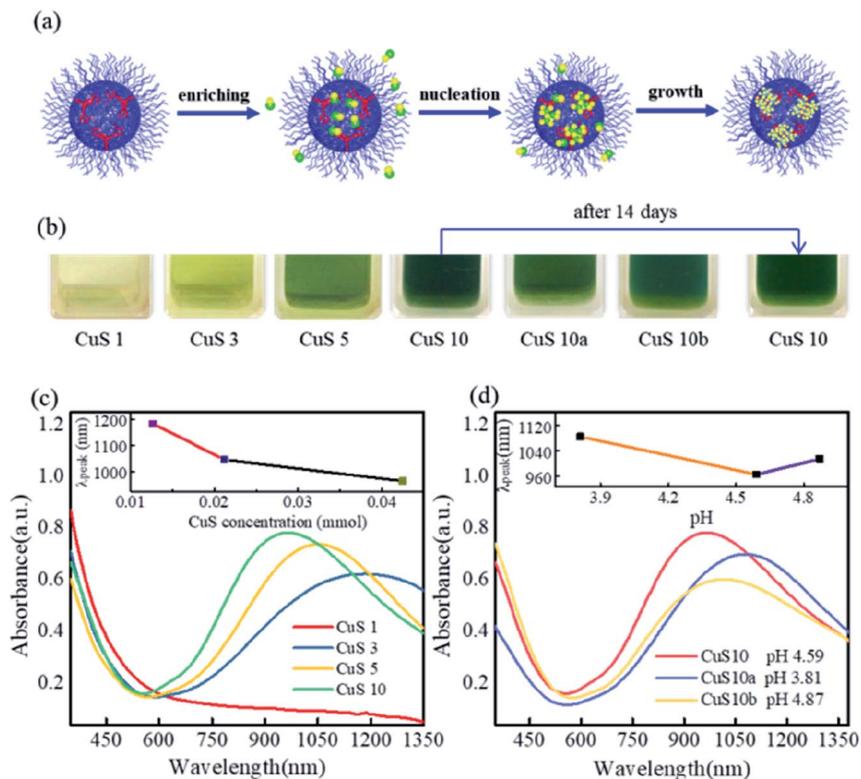
Fig. 2 (a) The illustration of the formation process of CuS nanocrystals using microgels as micro/nano reactors; (b) the photographs of the origin solutions of poly(VCL-co-MAA)@CuS1, 3, 5, 10, 10a, and 10b hybrid microgels (short form: CuS1, CuS3, CuS5, CuS10, CuS10a, and CuS10b, respectively); the UV-vis absorbance spectra of hybrid microgels synthesized with varying feeding molar ratios of Cu and −COOH from 1 : 2 to 1 : 20 (c) and poly(VCL-co-MAA)@CuS10, 10a, and 10b (d).

the decreased intensity. In the SEM image of poly(VCL-co-MAA)@CuS10a in Fig. S10a,† a large amount of aggregated nanocrystals could be found outside the microgels. This observation indicated that the formation of nanocrystals might occur outside the microgels under acidic conditions, as a result of less Cu^{2+} ions being enriched within the microgels. Furthermore, the inorganic structure was identified as covellite CuS nanocrystals by X-ray diffraction, as shown in Fig. S11.† Based on the calculation from the diffraction peak width, the size of nanocrystals was roughly identified as 6.8 nm, which was much smaller than that for poly(VCL-co-MAA)@CuS10. The decrease in size might mainly be the cause of the red-shift of the absorption spectrum.

On the other hand, the poly(VCL-co-MAA)@CuS10b sample synthesized with excess base tended to be black and showed relatively poor colloidal stability. One possible reason for such a red-shift in the absorption spectrum might be that Cu(ɪɪ) ions might precipitate in the form of $Cu(OH)_2$ after the addition of 50 μL of NaOH solution. According to the solubility product of $Cu(OH)_2$ ($K_{sp,Cu(OH)_2} = 10^{-19.6}$), the upper value of the pH for the occurrence of precipitation was 5.23. In this case, the pH of the solution was 5.20, smaller than 5.23. So Cu(ɪɪ) elements here would still exist as cations.

Another possible reason is that the carboxyl groups inside the microgels might deprotonate to a greater degree since the full deprotonation of carboxyl groups occurred at a pH of 8.0 (as

presented in Fig. S1†). In that way, the addition of base led to the adsorption of Cu(ɪɪ) ions into microgels, and further facilitated the nucleation of nanocrystals and finally caused the smaller crystal sizes. To investigate the details, SEM and XRD detection also were utilized and the results are given in Fig. S10b and S11,† respectively. SEM images showed spherical structures as microgels and bare crystals could be found outside the microgels. The XRD pattern identified the inorganic component as covellite CuS nanocrystals. The calculated size of nanocrystals from the diffraction peak width was roughly identified as 2.5 nm, also smaller than that of poly(VCL-co-MAA)@CuS10 hybrid microgels. Despite the details of sizes from XRD data being inaccurate, the relative comparison between them still indicated that the smaller sizes of nanocrystals might be the reason for the red-shift in the absorption spectra.

The pH response of plasmon resonance for the as-synthesized poly(VCL-co-MAA)@CuS10 hybrid microgel dispersion was recorded and is shown in Fig. S12.† The absorption peak was red-shifted from 965 nm to 974 nm as the pH values were adjusted from 5.54 to 10.09, along with the decreased intensity and the weakened color. These results indicated that pH values affected not only the enrichment of the CuS precursor within the microgels, but also the formation and stability of CuS nanocrystals.

CuS nanocrystals have attracted extensive attention in biomedicine due to their low cytotoxicity, strong near-infrared
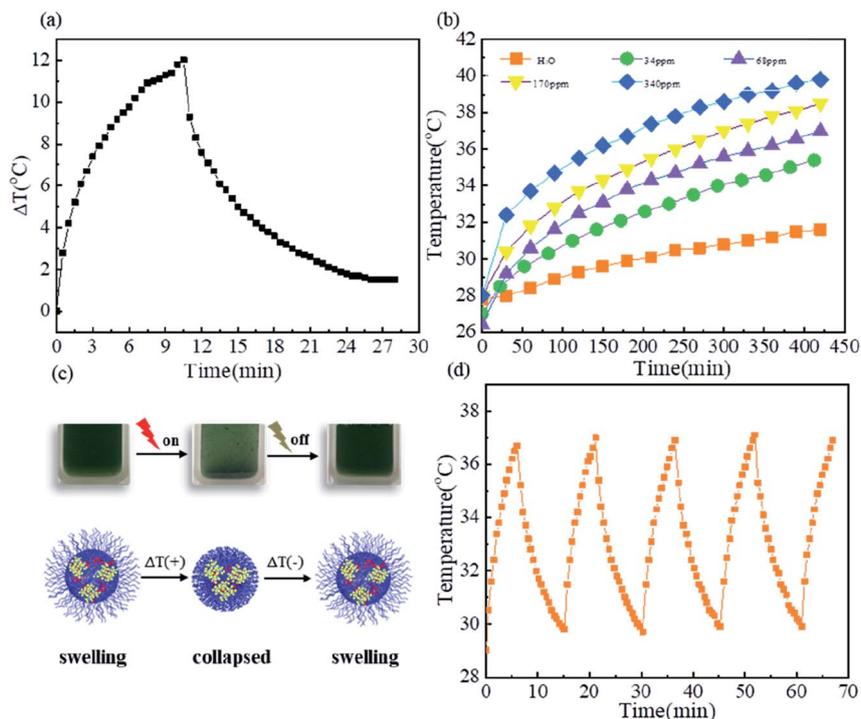
Fig. 3 (a) Photothermal effect of poly(VCL-*co*-MAA)@CuS10 hybrid microgels dispersed in aqueous solution (Cu content: 68 ppm) when illuminated with a 980 nm laser (0.67 W cm^{-2}). The laser was turned off after irradiation for 10 min; (b) temperature profile of ultrapure water and poly(VCL-*co*-MAA)@CuS10 hybrid microgels dispersed in aqueous solution at different CuS concentrations as a function of irradiation time; (c) schematic diagram of photothermal conversion of hybrid microgels; (d) temperature profile of poly(VCL-*co*-MAA)@CuS10 dispersed in aqueous solution at a CuS concentration of 68 ppm during five ON/OFF cycles of 980 nm NIR laser irradiation (0.67 W cm^{-2}).

absorption and high photothermal conversion efficiency. Here, we investigated the photothermal conversion of CuS nanocrystals for their potential application in remote near infrared-triggered release of drugs. Fig. 3a shows the photothermal effect of poly(VCL-*co*-MAA)@CuS10 dispersed in aqueous solution at a CuS concentration of 68 ppm under the irradiation of a 980 nm NIR laser. The maximum temperature change could reach up to 12 °C within the irradiation time of 10 min, indicating an effective photothermal conversion. However, a quantitative analysis of photothermal performance was much more difficult due to the collapse and aggregation of microgels at temperatures above their VPTT (see Fig. S8†).

The effect of CuS concentration on photothermal conversion was investigated at a series of concentrations ranging from 34 ppm to 340 ppm under 980 nm NIR laser irradiation for 7 min, and the results are shown in Fig. 3b. As the concentration increased from 34 ppm to 340 ppm, the initial heating rates rapidly increased and the maximum temperature change increased from 8 °C to 12 °C. The increase in temperature caused the dehydration of microgels, and the dehydration of microgels in turn switched off the photothermal conversion of CuS nanocrystals, as illustrated in Fig. 3c. The recyclability of this process was evaluated using five ON/OFF cycles under 980 nm NIR laser irradiation (0.67 W cm^{-2}) at a CuS concentration of 68 ppm, and the results are presented in Fig. 3d. Fig. 3d shows an extremely similar temperature profile as a function of irradiation time in each cycle, indicating their

excellent recyclability. These characteristics indicated that hybrid microgels could be promising potential candidates in the remote near infrared-triggered release of drugs without unexpected harm to normal tissues.

Conclusions

We reported a novel method for fabricating hybrid nanostructures to integrate thermoresponsive microgels and plasmonic semiconductor nanocrystals *via* the thermal synthesis of CuS nanocrystals within poly(*N*-vinyl caprolactam-*co*-methacrylic acid) microgels. In such a process, the microgel matrix provided a confined space and the carboxyl groups inside the microgels functioned as localized ligands for the formation of flake-like covellite CuS nanocrystals. The CuS nanocrystals showed strong adjustable NIR absorption spectra and different sizes *via* the modulation of synthesis parameters such as the content of CuS precursors and the pH of the medium. Even though further investigation of the nanocrystal formation mechanism is still needed, the introduced method emphasizes the importance of the roles of microgels and the use of ethanol under the conditions of high temperature, which will offer an alternative for the fabrication of hybrid nanostructures. Furthermore, the as-synthesized hybrid microgels exhibited good photothermal performance and thus could be one of the promising hybrid materials for the remote near infrared-triggered release of drugs in cancer therapy.

Conflicts of interest

The authors declare no competing financial interests.

Acknowledgements

References

1 A. Agrawal, S. H. Cho, O. Zandi, S. Ghosh, R. W. Johns and D. J. Milliron, *Chem. Rev.*, 2018, **118**, 3121–3207.

2 C. Coughlan, M. Ibanez, O. Dobrozhan, A. Singh, A. Cabot and K. M. Ryan, *Chem. Rev.*, 2017, **117**, 5865–6109.

3 S. Goel, F. Chen and W. B. Cai, *Small*, 2014, **10**, 631–645.

4 C. B. Williamson, D. R. Nevers, T. Hanrath and R. D. Robinson, *J. Am. Chem. Soc.*, 2015, **137**, 15843–15851.

5 M. Zhou, J. J. Li, S. Liang, A. K. Sood, D. Liang and C. Li, *ACS Nano*, 2015, **9**, 7085–7096.

6 G. Ku, M. Zhou, S. L. Song, Q. Huang, J. Hazle and C. Li, *ACS Nano*, 2012, **6**, 7489–7496.

7 M. A. C. Stuart, W. T. S. Huck, J. Genzer, M. Muller, C. Ober, M. Stamm, G. B. Sukhorukov, I. Szleifer, V. V. Tsukruk, M. Urban, F. Winnik, S. Zauscher, I. Luzinov and S. Minko, *Nat. Mater.*, 2010, **9**, 101–113.

8 J. Yang, S. D. Zhai, H. Qin, H. Yan, D. Xing and X. L. Hu, *Biomaterials*, 2018, **176**, 1–12.

9 T. Alejo, V. Andreu, G. Mendoza, V. Sebastian and M. Arruebo, *J. Colloid Interface Sci.*, 2018, **523**, 234–244.

10 J. Ramos, A. Imaz and J. Forcada, *Polym. Chem.*, 2012, **3**, 852–856.

11 J. Sun, R. Gui, H. Jin, N. Li and X. Wang, *RSC Adv.*, 2016, **6**, 8722–8728.

12 J. G. Zhang, S. Q. Xu and E. Kumacheva, *J. Am. Chem. Soc.*, 2004, **126**, 7908–7914.

13 A. Pich, J. Hain, Y. Lu, V. Boyko, Y. Prots and H. J. Adler, *Macromolecules*, 2005, **38**, 6610–6619.

14 W. T. Wu, T. Zhou, M. Aiello and S. Q. Zhou, *Biosens. Bioelectron.*, 2010, **25**, 2603–2610.

15 W. T. Wu, T. Zhou, J. Shen and S. Q. Zhou, *Chem. Commun.*, 2009, **29**, 4390–4392.

16 M. Agrawal, A. Pich, S. Gupta, N. E. Zafeiropoulos, J. Rubio-Retama, F. Simon and M. Stamm, *J. Mater. Chem.*, 2008, **18**, 2581–2586.

17 T. Shu, Q. M. Shen, L. Su, X. J. Zhang and M. J. Serpe, *ACS Appl. Nano Mater.*, 2018, **1**, 1776–1783.

18 S. Backes, P. Krause, W. Tabaka, M. U. Witt, D. Mukherji, K. Kremer and R. von Klitzing, *ACS Macro Lett.*, 2017, **6**, 1042–1046.

19 J. Peng, D. Y. Tang, S. Y. Jia, Y. Zhang, Z. J. Sun, X. Yang, H. Y. Zou and H. T. Lv, *Colloid. Surface. Physicochem. Eng. Aspect.*, 2019, **563**, 130–140.

20 W. J. Lin, X. M. Ma, J. S. Qian, A. I. Abdelrahman, A. Halupa, V. Baranov, A. Pich and M. A. Winnik, *Langmuir*, 2011, **27**, 7265–7275.

21 S. Thies, P. Simon, I. Zelenina, L. Mertens and A. Pich, *Small*, 2018, **14**, 7.

22 D. L. Perry and J. A. Taylor, *J. Mater. Sci. Lett.*, 1986, **5**, 384–386.

23 Y. Xie, A. Riedinger, M. Prato, A. Casu, A. Genovese, P. Guardia, S. Sottini, C. Sangregorio, K. Miszta, S. Ghosh, T. Pellegrino and L. Manna, *J. Am. Chem. Soc.*, 2013, **135**, 17630–17637.

24 S.-W. Hsu, C. Ngo and A. R. Tao, *Nano Lett.*, 2014, **14**, 2372–2380.

25 B. Li, Q. Wang, R. Zou, X. Liu, K. Xu, W. Li and J. Hu, *Nanoscale*, 2014, **6**, 3274–3282.